13

C-band Scatterometers and Their Applications

Vahid Naeimi and Wolfgang Wagner
Vienna University of Technology
Austria

1. Introduction

Scatterometers are non-imaging active sensors used to measure the intensity of microwave backscatter while scanning the surface of the earth from an aircraft or a satellite. Active microwave sensors are radars providing their own illumination and do not depend upon ambient radiation like passive microwave sensors. They transmit microwave electromagnetic pulses toward the surface and measure how much of that signals return after interacting with the target. Scatterometer is a form of radar that is used to investigate different geophysical properties of the surface and few centimeters beneath. Spaceborne scatterometers have the advantage of providing global coverage on a continuous basis, which cannot be achieved through airborne or ground measurements. They have the capability of providing day and night time measurements unaffected by cloud cover. Scatterometers were originally designed to study ocean winds but have been also used to study of cryosphere, vegetation, and soil surface properties.
A number of scatterometers have been flown on space missions since the early 1970s. The first scatterometer in space was a Ku-band instrument on Skylab mission. Investigations on the potential use of scatterometers in geosciences achieved a major technical milestone with the launch of Seasat, carrying a Ku-band scatterometer (SASS), in 1978. Other missions have followed SASS; C-band scatterometers onboard the European Space Agency's (ESA) Earth Remote Sensing (ERS 1 & ERS-2) satellites in 1991 and 1995, the NASA's Ku-band scatterometer (NSCAT) in 1996, SeaWinds on QuikSCAT in 1999, SeaWinds on ADEOS-II in 2002, and Advanced Scatterometer (ASCAT) onboard Metop-A launched in 2006.
In this study we focus on spaceborne C-band scatterometers and present an overview of their applications in geoscience.

2. C-band Scatterometers

2.1 SCAT onboard ERS satellites

The first spaceborne C-band scatterometer was flown on ERS-1, the European Earth observation mission. ERS-1, launched in July 1991, was aimed to provide environmental monitoring particularly in the microwave spectrum. ERS-1 has been placed in a near-polar orbit at a mean altitude of about 780km with an instrument payload comprising active and passive microwave sensors and a thermal infra-red radiometer. ERS-2 the follow-up ESA mission of ERS-1 was launched in 1995. The ERS-2 satellite is a copy of ERS-1 except that it

includes a number of enhancements and new payload instruments. Both scatterometers onboard ERS-1 and ERS-2 are part of an Active Microwave Instrument (AMI) operating in C-band (5.3 GHz). The AMI incorporates two separate radar systems; Synthetic Aperture Radar (SAR) and scatterometer (SCAT) operating in three different modes. SAR for Image and Wave mode operations, and scatterometer for Wind mode operation. The Wind and Wave modes are capable of interleaved operation, i.e. so-called Wind/Wave mode, but the operation in Image mode excludes the operation of the other two modes (Attema, 1991).

2.2 ASCAT onboard Metop satellites

The Advanced Scatterometer (ASCAT) is the new generation and successor of the ERS SCATs onboard the Meteorological Operational (Metop) series of satellites. Metop-A, launched on 19 October 2006, is the first satellite in the series foreseen in EUMETSAT Polar System (EPS) program (Klaes et al., 2007). Like SCAT, ASCAT system uses a fan-beam antenna technology and transmits vertically polarized pulses at frequency of 5.255 GHz with high radiometric stability. Contrary to SCAT it uses two sets of three antennas instead

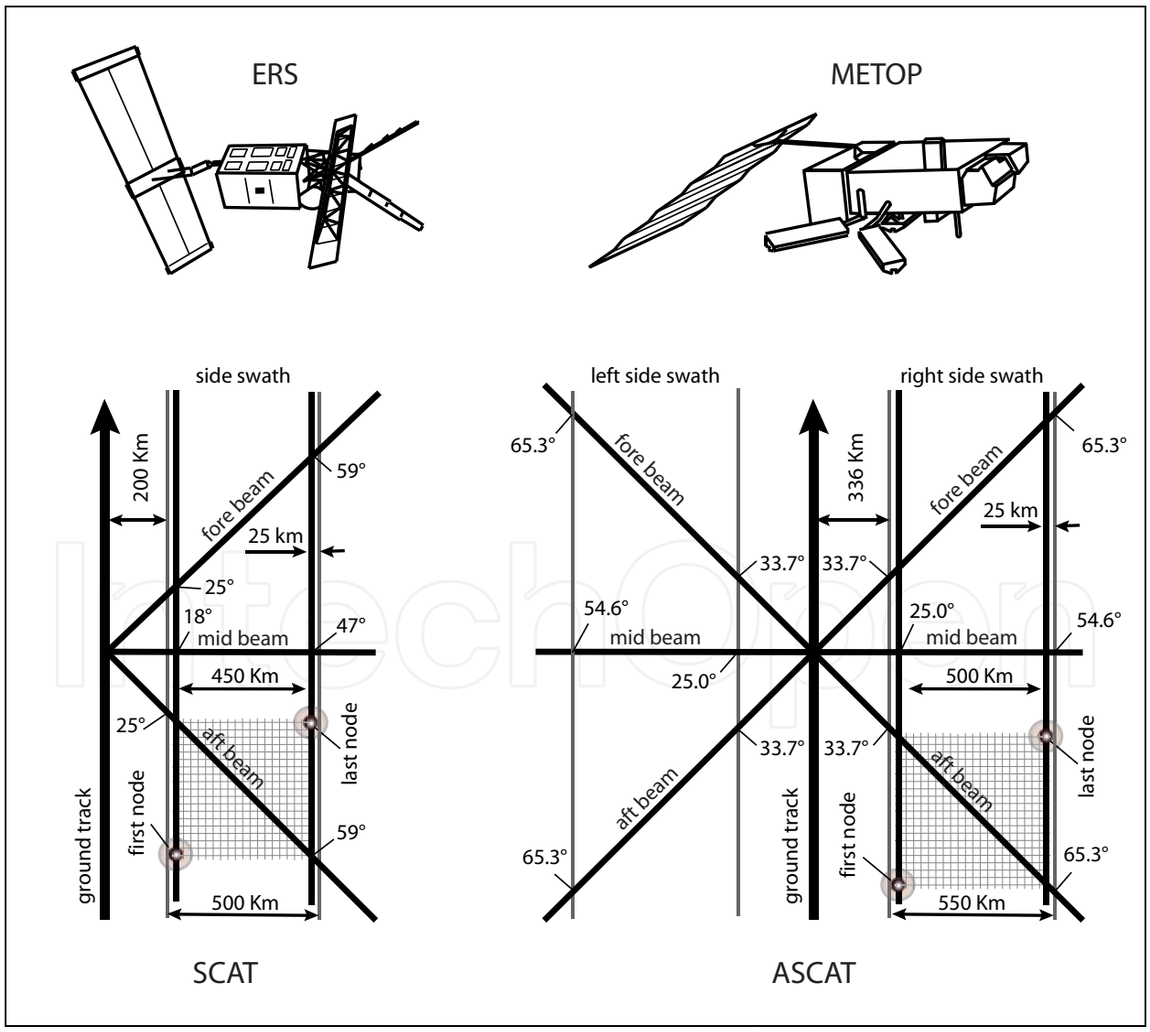

Fig. 1. Viewing geometries of the scatterometers onboard ERS and Metop satellites.

of one. For ASCAT the incidence angle range has been extended from 25° to 65°. Hence ASCAT covers two 550 km swaths to the left and right of the satellite ground track which are separated from the satellite ground track by about 336 km. This results in over twice faster global-coverage capability than its predecessor SCAT. Beside an optimized viewing geometry, ASCAT also features a number of technical improvements. The improved instrument design and radiometric performance results in higher stability and reliability of ASCAT measurements. Additionally EUMETSAT foresees to generate a research product at a resolution of 25km (Figa-Saldana et al., 2002). Figure 1 illustrates the viewing geometries of SCAT and ASCAT. Specifications of the C-band scatterometers and their carrier satellites are given in table-1.

Satellite Specifications	**ERS-1**	**ERS-2**	**Metop-A**
Launch Time	17 July 1991	21 April 1995	19 October 2006
Launch Mass	2354 kg	2516 kg	4093 kg
launcher	Ariane 4		Soyuz/ST
Spacecraft Altitude	770 to 785 km		800 to 850 km
Inclination	98.52°		98.7°
Local Solar Time	10:30 am*		9:30 am*
Orbit Period	100 minutes		101 minutes
Orbit	Near-circular, polar, Sun-synchronous		
Scatterometer Specifications	**SCAT**		**ASCAT**
Frequency	5.3 GHz. (C-Band)		5.255 GHz. (C-Band)
Polarization	VV		VV
Swath Width	500 km		550 km (double swath)
Swath Stand-off	200 km to the right of sub-satellite track		336 km
Localization Accuracy	5 km		4.4 km
Spatial Resolution	50 km		50 km, 25 km
Sampling Interval	25 km		25 km, 12.5 km
* equatorial crossing time at the descending node			

Table 1. Specifications of the European C-band scatterometers

3. Wind Speed and Direction Measurement

The primary application of the spaceborne scatterometry has been the measurement of near-surface winds over the ocean. The concept of retrieving wind speed at sea surface from the radar backscatter goes back to the Second World War. During the World War II, marine radar operators observed disturbing noises, called "*clutter*", on their radar screens, which made them difficult detecting targets on the ocean surface (Moore et al., 1979). The clutters were the backscatter of the radar pulses from the small waves on the sea surface. Since that time many theoretical studies and experiments have been carried out to find the relationship between the microwave backscatter and the surface wind speed (Liu, 2002). The idea of remote sensing of the wind relies on the fact that winds over the sea cause small-scale disturbances of the sea surface which modify the radar backscattering characteristics. The backscatter from oceans is largely due to these small centimeter ripples, capillary waves, which is in equilibrium with the local wind stress. The backscatter depends not only on the magnitude of the wind stress but also the wind direction relative to the direction of the

radar beam. By combining backscatter measurements from different azimuth angles, the near-surface wind vector over the ocean's surface can be determined using a Geophysical Model Function (GMF). The first operational GMF used for ERS-1 scatterometer data by ESA was a prelaunch transfer function denoted CMOD2, derived from aircraft-mounted instrument data (Long, 1985). An improved transfer function, CMOD4 was presented by Stoffelen et al. (1997) with full specification. CMOD4 adopted by ESA since March 1993 for wind retrieval. The latest C-band GMF used for wind retrieval is CMOD5, which is derived on the basis of measurements from the ERS-2 scatterometer. The CMOD5 algorithm corrects some shortcomings in the earlier models and result in a better wind retrieval at high wind speed and more uniform performance across the scatterometer swath (Hersbach et al., 2007). The estimated accuracy of the ASCAT 50-km wind product is 2 m/s RMS difference in wind vector components and 0.5 m/s bias in wind speed (ASCAT product guide). The wind observations at sea surface are essential to describe the atmospheric flow and therefore have many meteorological and oceanographic applications. Wind information is useful for weather forecasting, prediction of extreme events, and climate studies. Figure 2 indicates two examples of the ASCAT 25- and 12.5-km wind products (Verhoef et al., 2009). Processing of the wind product is done in near-real time at EUMETSAT's processing facility. From the sensing time, it takes approximately 2 hours to get the corresponding wind product ready at KNMI. The wind data are disseminated through the EUMETCast system (EUMETCast).

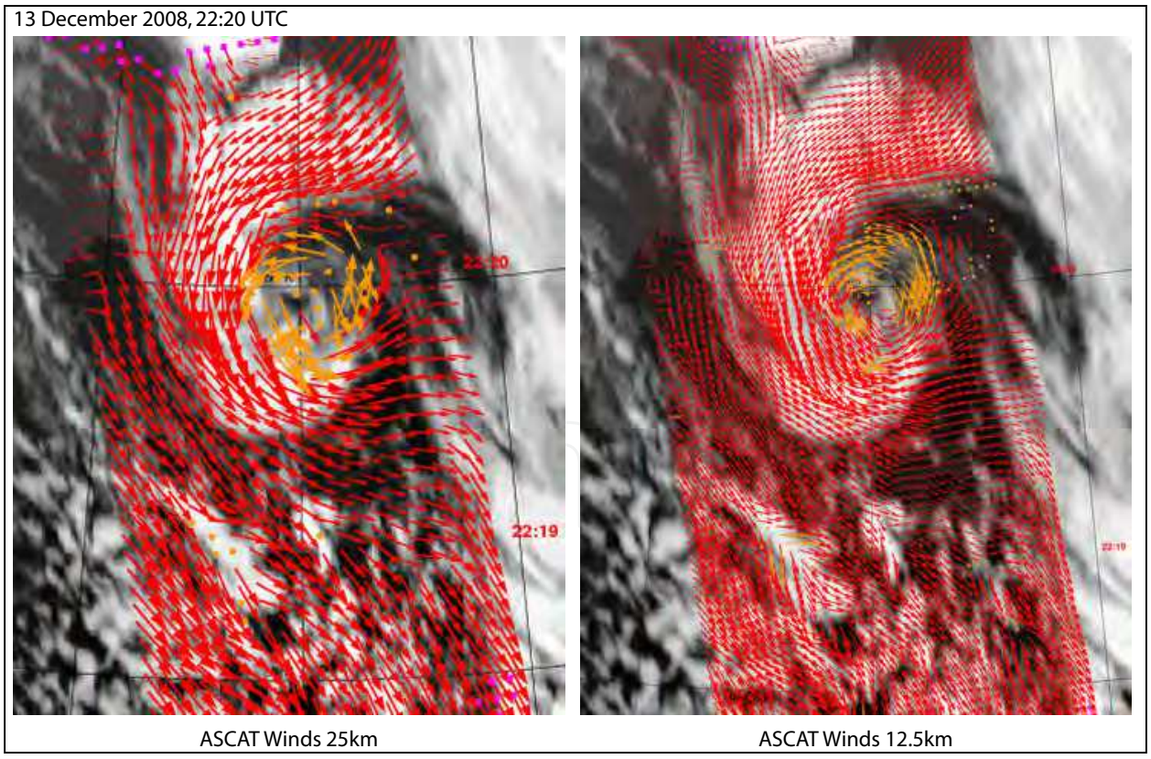

Fig. 2. ASCAT wind product over Atlantic Ocean (55°N-65°N, ~15° West, South of Iceland). Background image shows the infrared cloud image of the METEOSAT9 geostationary satellite. Images are adopted from (Verhoef et al., 2009).

4. Monitoring Seasonal Dynamics of Vegetation

The intensity of the backscattered signal over land is affected by roughness, vegetation structure, vegetation water content, and soil moisture. These factors influence the backscattering coefficient σ^0 on different time scales. At the resolution of the ERS and Metop scatterometers, surface roughness can be in general considered as a temporally invariant parameter. Surface soil moisture changes rapidly within hours to days, contrary to the vegetation canopy and vegetation water content, which vary within several days to weeks. Scattering from the vegetated surface is a complex phenomenon and difficult to model as the volume scattering contributes in total backscattering. Preliminary studies indicated the potential of the C-band scatterometer data for monitoring the seasonal variation of vegetation using multi-temporal analysis (Wismann et al., 1994; Mougin et al., 1995; Frison et al., 1996a; Frison et al., 1996b). Many studies used semi-empirical models to model vegetation effect on backscatter (Magagi et al., 1997; Woodhouse et al., 2000; Jarlan et al., 2003). There have been several canopy scattering models developed to describe σ^0 in terms of vegetation and soil surface parameters based on a solution of the radiative transfer equation (Attema et al., 1978; Ulaby et al., 1990; Karam et al., 1992; Saatchi et al., 1994). Radiative transfer theory describes the propagation of radiation through a medium affected by absorption, emission and scattering processes (Fung, 1994). But the problem with all complex theoretical scattering models is that their input data requirements are very challenging and for solving the equations many parameters are needed such as leaf diameter, branch length, trunk moisture, and probability functions representing the orientational distribution of leaves, branches, and trunks.

The incidence angle of scatterometer observations varies from acquisition to acquisition. Since the intensity of backscatter signal strongly depends on the incidence angle, in the most of the multi-temporal vegetation studies using scatterometer data, σ^0 measurements are averaged over longer periods (e.g. one month) to make σ^0 measurements comparable. But the averaging procedure does not allow us to distinguish the impact of the soil moisture and vegetation cover on backscatter. Wagner et al. (1999a) used a simple model fitted to scatterometer observations to model the incidence angle dependency of backscatter:

$$\sigma'(\theta) = \frac{d\sigma^0(\theta)}{d\theta} \tag{1}$$

σ' shows the incidence angle dependency of σ^0. Knowing the incidence angle dependency, σ^0 can be normalized at a reference incidence angle. In this approach σ' is calculated for each triplet, which contains concurrent measurements representing the same soil moisture condition. Therefore the effect of soil moisture on incidence angle behavior of σ^0 is negligible, if not completely removed from the backscattered signal:

$$\sigma'\left(\frac{\theta_m - \theta_{a/f}}{2}\right) = \frac{\sigma^0_m(\theta_m) - \sigma^0_{a/f}(\theta_{a/f})}{\theta_m - \theta_{a/f}} \tag{2}$$

where the index *m* stands for the mid-beam and the indices *a* and *f* for the aft and fore beam measurements.

The backscattered energy received by the scatterometer sensor increases with decreasing incidence angle. The rate of backscatter change due to incidence angle variation depends on the surface roughness. Bare soil roughness is basically constant in time but vegetation can have a seasonal influence on the incidence angle dependency behavior of backscatter. With increasing vegetation density, the shape of incidence angle dependency of backscatter changes depending on the type and density of vegetation as well as the orientation of vegetation elements. Having multi-year scatterometer data, the seasonal variation of slope can be extracted for a reference incidence angle (e.g. 40°). Slope function at 40°, $\sigma'(40)$ correlates pretty well with the seasonal vegetation change (Naeimi et al., 2009a). Figure 3-top shows slope values globally calculated for the mid of July. Figure 3-bottom illustrates three examples of $\sigma'(40)$ from different regions compared with the Normalized Vegetation index (NDVI). The vegetation index data have been derived from a 16-day Moderate Resolution Imaging Spectroradiometer (MODIS) NDVI product (Huete et al., 2002). NDVI

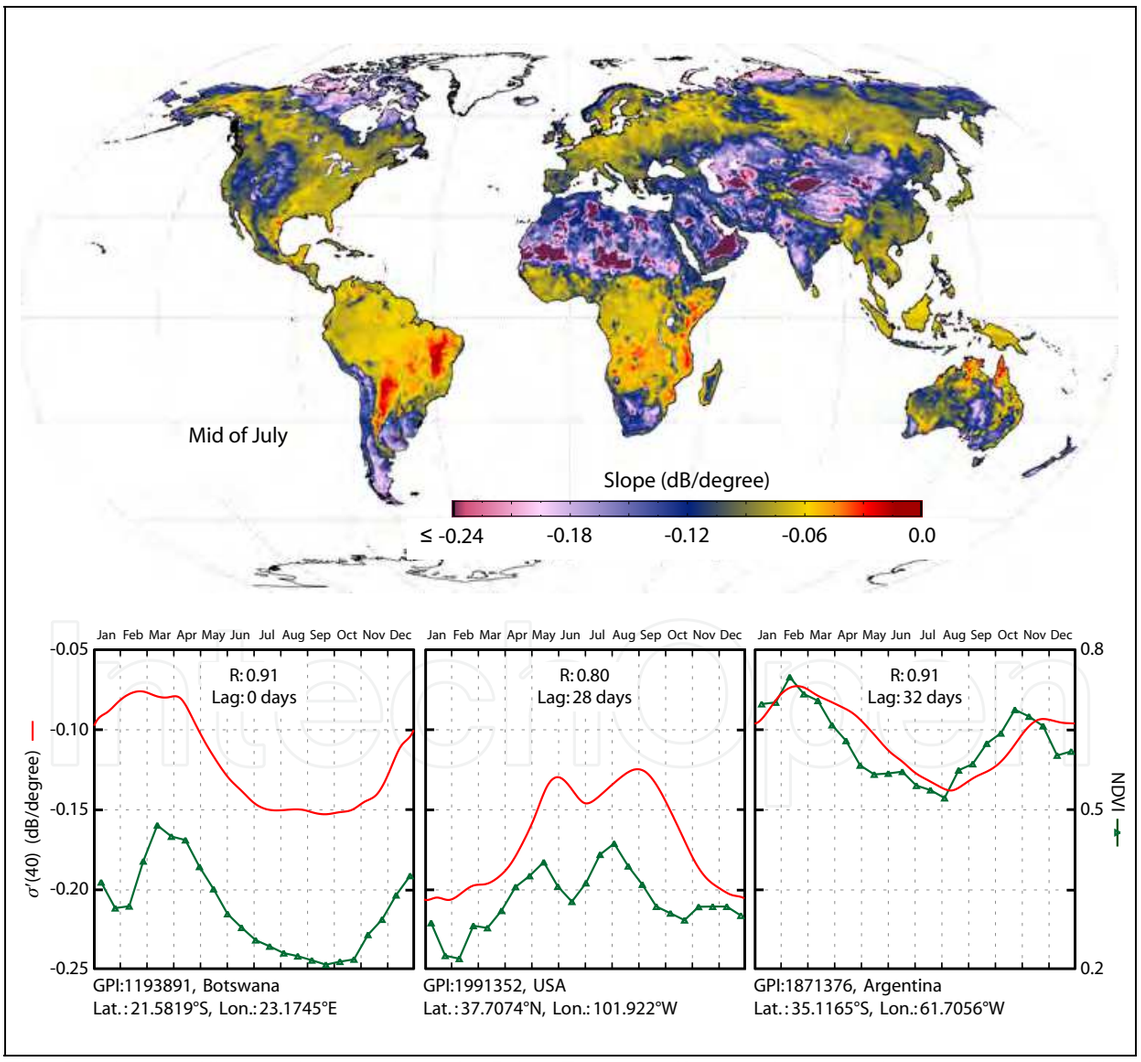

Fig. 3. Above: Global slope values in July. Bottom: Comparison of slope function with NDVI in three different areas.

values are averaged over three years (2000–2002) to estimate the yearly vegetation variation. Depending on land cover type there is a time lag between NDVI and $\sigma'(40)$ in most regions (Doubkova et al., 2009). This implies the fact that the σ' derived from C-band backscatter observations corresponds to vegetation structure development whereas NDVI represents only greenness of vegetation canopy.

5. Soil Moisture Change Detection

As it mentioned in section 4, σ^0 is affected over land by surface roughness, vegetation, and soil moisture. The major challenge of extracting soil moisture from scatterometer data is the presence of the other additional factors influencing the signal. Most studies have introduced physical inversion methods describing scattering process to model roughness and vegetation contributions on backscatter signal (Frison et al., 1997; Pulliainen et al., 1998; Woodhouse et al., 2000; Magagi et al., 2001; Jarlan et al., 2002; Zine et al., 2005). Although theoretical models are useful for understanding and interpreting scattering behavior of natural surfaces, the major problems of these retrieval concepts appear to be their complexity and physical validity at large scales. A promising solution to the problems of physically based inversion models is using change detection method rather than using a complex model to describe the full range of parameters influencing the scattering process. Availability of several years of backscatter data, multi-viewing capability, and high temporal sampling rate of scatterometers make them appropriate instruments for change detection methods. The potential of using change detection techniques for active sensors has been demonstrated in several studies (Wagner, 1998, Moeremans et al., 1998, Quesney et al., 2000; Moran et al., 2000; Le Hegarat-Mascle et al., 2002; De Ridder, 2000).

5.1 TUWien change detection method

Wagner et al., (1999b) presented a change detection method for soil moisture retrieval from ERS scatterometers. A processing algorithm for soil moisture retrieval based on change detection technique has been developed at the Institute of Photogrammetry and Remote Sensing (IPF) of the Vienna University of Technology (TUWien) which will further be referred to as the TUWien method. In the TUWien method soil moisture dynamics are extracted after modeling the behavior of σ^0 with respect to the surface roughness and the local variability of vegetation and eventually subtracting them from the backscatter signal. In the retrieval algorithm, multi-looking direction ability of scatterometer is used to describe the incidence angle behavior of the backscatter signal as a seasonal function, $\sigma'(\theta)$. The incidence angle dependency of backscatter can be described by the derivatives of σ^0 at a reference incidence angle (set to 40°) according to the Taylor series expansion:

$$\sigma'(\theta) = \sigma'(40) + \sigma''(40)(\theta - 40) \tag{3}$$

$\sigma'(40)$ and $\sigma''(40)$, called slope and curvature at 40°, are calculated by fitting a regression line to the obtained local slope values in equation-2 during a certain period of the year. After determination of slope and curvature for each day of year and using the following second-

order polynomial equation based on Taylor series, $\sigma^0(\theta)$ measurements are extrapolated to 40° incidence angle:

$$\sigma^0(40) = \sigma^0(\theta) - \sigma'(40)(\theta - 40) - \frac{1}{2}\sigma''(40)(\theta - 40)^2 \quad (4)$$

Eventually the normalized backscatter $\sigma^0(40)$ is scaled between the lowest and highest values ever measured within the long-term $\sigma^0(40)$ observations, $\sigma^0_{wet}(40)$ and $\sigma^0_{dry}(40)$, which represent the driest and wettest conditions:

$$\Theta_s = \frac{\sigma^0(40) - \sigma^0_{dry}(40)}{\sigma^0_{wet}(40) - \sigma^0_{dry}(40)} \times 100 \quad (5)$$

Θ_s corresponds to the normalized volumetric water content at topmost 2 cm soil surface ranging between 0% and 100% with presumption of linear relationship between $\sigma^0(40)$ and the surface soil moisture (Ulaby et al., 1982). In addition the TUWien retrieval algorithm includes processing modules for vegetation correction, wet reference correction and soil moisture uncertainty analysis (Naeimi et al., 2009a). An operational processing system based on the TUWien retrieval algorithm is implemented at EUMETSAT to provide near-real time ASCAT soil moisture data (Hasenauer et al., 2006). The data have been made available through the EUMETCast system (EUMETCast). Figure 4 shows SCAT/ASCAT soil moisture time series compared with precipitation data at a grid point located in Lower Austria. An example of global distribution of the mean soil moisture values retrieved from long-term SCAT time series is shown in Figure 5. The spatial variability of the estimated mean of soil moisture is connected to atmospheric-forcing related soil moisture signal. Soil moisture retrieval from scatterometer data has also limitations when the soil is frozen or

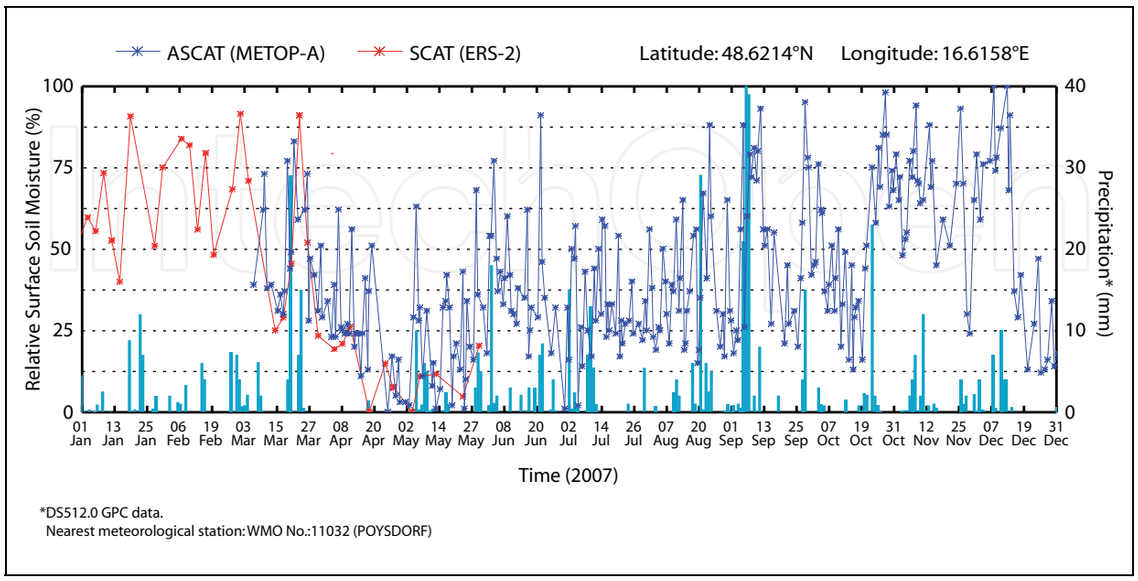

Fig. 4. Soil moisture time series retrieved from SCAT and ASCAT data compared with precipitation data in lower Austria.

covered with snow. As soon as the soil freezes the dielectric constant of the soil drops drastically and results in low backscatter. Therefore the backscattering behaviors of dry and frozen soil are similar. The scattering behavior of snow is more complex and depends on the dielectric properties of the ice particles and on their distribution and density. Furthermore, land cover has also impacts on the quality of soil moisture retrieval from scatterometer data. There is a strong response of the azimuthal noise level of backscatter to different land cover types like rainforests, lakes, rivers, floodplains, coastal areas, urban areas, and sand deserts as well as areas with complex topography (Naeimi et al., 2008). An uncertainty analysis module using Monte Carlo error propagation (Naeimi, 2009b) is implemented within the TUWien algorithm which identifies such problematic areas for soil moisture retrieval from scatterometer data.

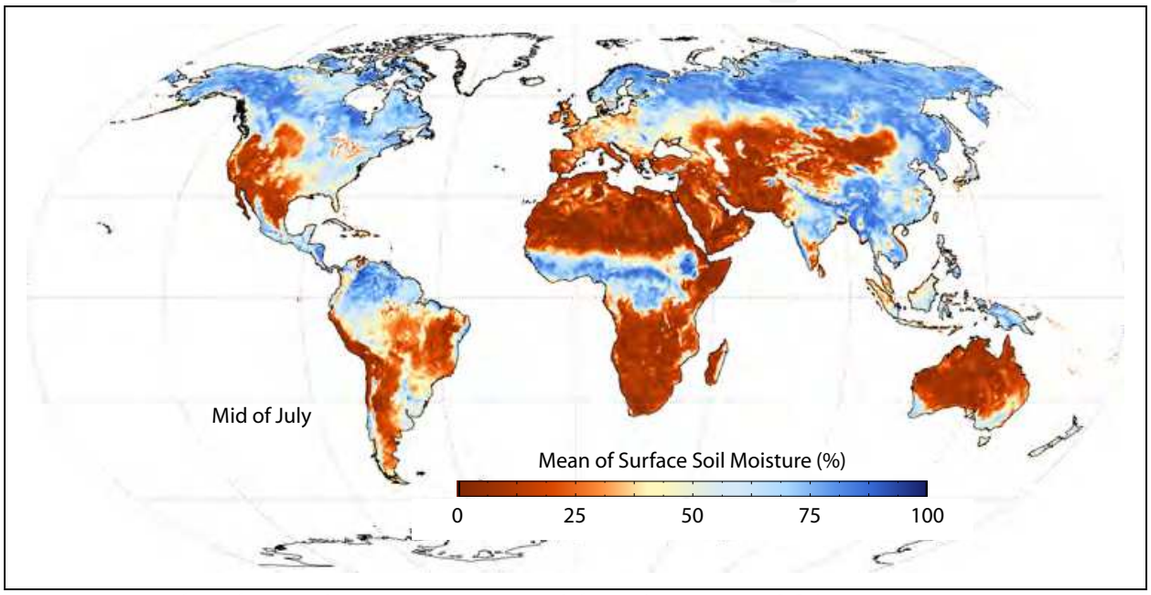

Fig. 5. Mean of surface soil moisture retrieved from long-term SCAT time series.

5.2 Surface soil moisture anomalies

Anomalies of soil moisture, precipitation, temperature, and vegetation indices are parameters that are used as indicator of extreme weather conditions. Scatterometer soil moisture anomalies can be calculated by comparing the current values with mean and standard deviation values in the same time of year over the long-term ERS/Metop scatterometer time series. Figure 6 illustrates monthly anomalies of ASCAT soil moisture compared with the NDVI anomaly images derived from MODIS data (NASA-EO). The extremely dry conditions are visible in parts of Europe during July 2007 (Figure 6-a). As reported by the authorities the 2007 drought in Moldova was the most severe in living memory. The World Food Program compared its severity to the drought of 1946 during which many Moldovans starved. The Cereal production at that year was down by 63% compared to the year before, and was about 70% lower than the average of the five years before (FAO news). Figure 6-b shows another example of extreme condition, which is evident in ASCAT soil moisture anomalies. The anomalous wet soil in March 2008 in parts

of India provided a suitable condition for vegetation growth. By early April 2008, plants throughout the country were responding to the plentiful water supply that led to record of harvest yield in April (NASA-EO).

5.3 Soil Water index (SWI)

The C-band scatterometer derived soil moisture represent only top few centimeter of soil. Nevertheless, thanks to the high temporal sampling of scatterometers (about 80% global daily coverage for ASCAT), soil moisture in plant root zone can be estimated by using an infiltration model. Wagner et al. (1999b) proposed a simple two-layer water balance model to estimate profile soil moisture. The remotely sensed topsoil represents the first layer and the second layer extends downwards from the bottom of the surface layer. In this model, the water content of the reservoir layer is described in terms of a Soil Water Index (SWI), which is controlled only by the past soil moisture conditions in the surface layer in a way that the influence of measurements decreases by increasing the time:

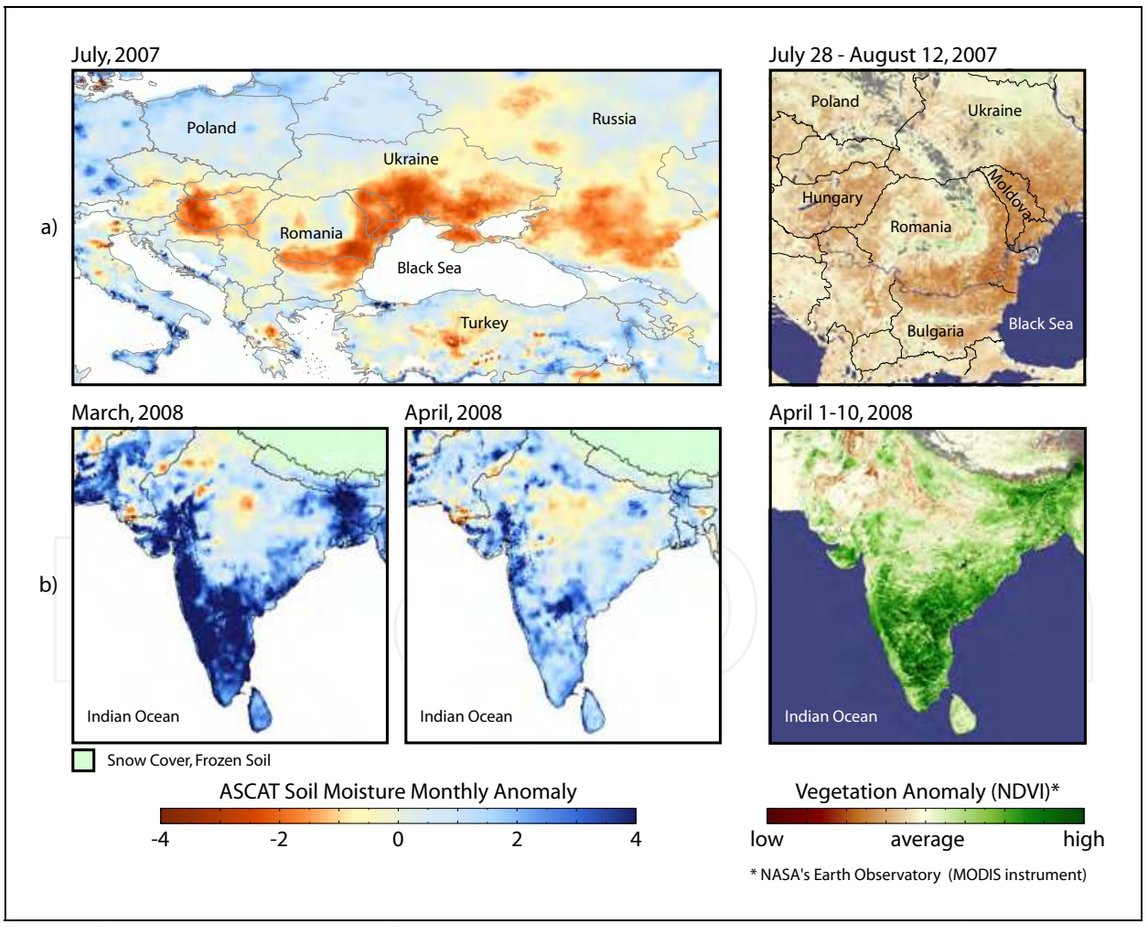

Fig. 6. Examples of the ASCAT soil moisture anomalies showing extreme dry (top) and wet conditions (bottom) compared with NDVI anomalies extracted from MODIS data.

$$SWI(t_n) = \frac{\sum_{i}^{n} \Theta_s(t_i) e^{-\frac{t_n - t_i}{T}}}{\sum_{i}^{n} e^{-\frac{t_n - t_i}{T}}} \quad for\ t_i \le t_n \tag{6}$$

$\Theta_s(t_i)$ is the surface soil moisture measured at time t_i and T is the characteristic time length connected to the depth of reservoir which describes the linkage between the surface layer and the reservoir by:

$$T = L/C \ , \quad L\frac{d\Theta(t)}{dt} = C \cdot \left[\Theta_s(t) - \Theta_r(t)\right] \tag{7}$$

where L is the depth of the reservoir layer and C is a pseudo-diffusivity coefficient that depends on soil properties. Θ_s and Θ_r are the volumetric moisture content of the surface and reservoir respectively.

Daily images of SWI calculated at five different T values (10, 20, 40, 60, 100) retrieved from ASCAT-25km observations using a near-real time recursive processor will be available through the geoland project (geoland-II). Figure 7 indicates the global ASCAT-50km SWI image calculated for T=10 as an example.

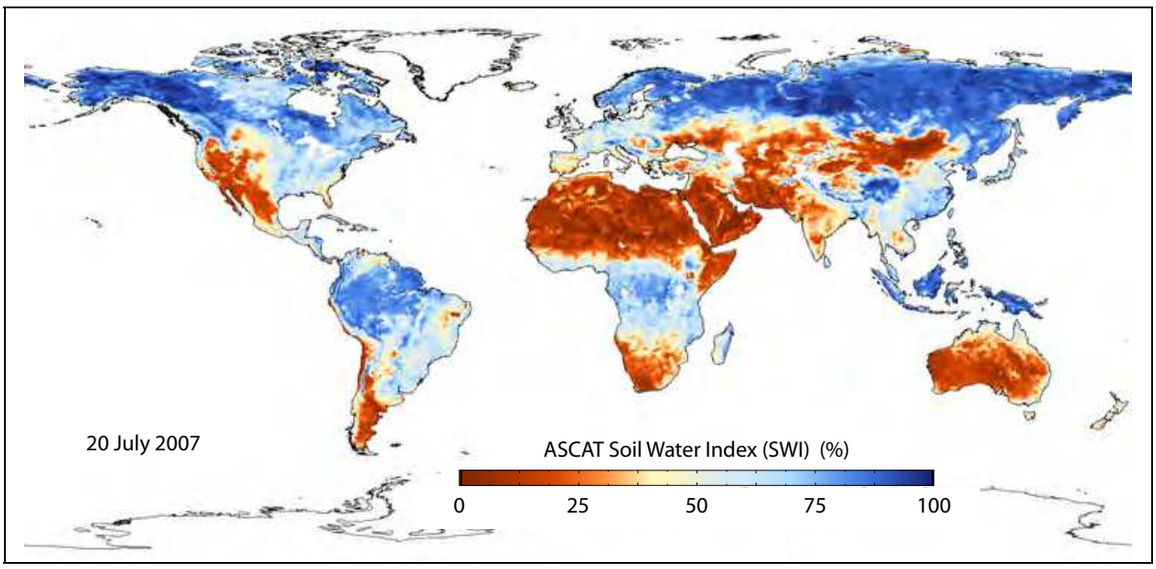

Fig. 7. ASCAT-50km Soil Water Index (SWI) at T=10.

6. Monitoring Cryosphere

The cryosphere consists of the parts of the Earth's surface where water exists in solid form, including snow cover, frozen ground, glacier, see ice, ice sheets and any other form of ice on land or in ocean. The cryosphere plays an important role in the global climate system and

therefore impacts significantly human life. More than about 70% of the Earth's freshwater is frozen in ocean ice sheets, glaciers or permafrost areas (UNESCO report, 2006). Permafrost regions are of major interest in climate studies as several hundred gigatons of carbon are stored in frozen soils in high latitudes. Thawing of permafrost could supercharge the global warming process. There is also a major concern about the possibility of shrinking the Earth's ice sheets due to the global warming which could raise the global sea level by several meters. There are many cryosphere-climate feedback mechanisms in the global climate system over a wide range of spatial and temporal scales. Snow and ice have a remarkable effect on climate as they modulate energy exchanges between the surface and the atmosphere because of their physical properties. One of the most important properties is the surface reflectance (albedo). Non-melting snow and ice can reflect between ~80-90% of incident solar energy whereas vegetation and soil surface reflect as little as 20-30%. The reflected sunlight into space does not get absorbed by the Earth as heat. Therefore the high albedo plays as a cooling factor in the global climate system. The thermal properties of cryospheric elements have also major consequences for the climate and hydrological cycle. Snow and ice have much lower thermal diffusivities than air and build an insulating layer over land and ocean surfaces decoupling the surface-atmosphere interface with respect to both heat and moisture fluxes. High latent heat is another thermal property of snow and ice that act to moderate temperature in warm seasons because of the large amount of energy required to melt ice.

Scatterometry has been proven to be useful for monitoring and understanding the cryosphere. Several studies have investigated the applicability of scatterometer data in various cryosphere research areas for instance; mapping snowmelt extent (Wismann et al., 1997; Wismann, 2000), snow accumulation in Greenland (Drinkwater et al., 2001), snow cover over the Northern Hemisphere (Nghiem et al., 2001), frozen terrain in Alaska (Kimball et al., 2001). Other studies have used scatterometer data for determination of freeze/thaw cycles in Northern Latitudes (Bartsch et al., 2007), spatial and temporal variability of sea ice (Drinkwater et al., 2000), classification of sea ice in Polar Regions (Remund et al., 2000), deriving the surface wind-induced patterns over Antarctica by measuring the azimuthal modulation of backscatter (Long et al., 2000).

In winter when soil surface freezes, dielectric properties of the soil changes significantly which results in low backscatter values. As snow begins to fall and accumulates over the surface, due to volume scattering, backscatter signals increase depending on microwave frequency. The response of dry snow volume to microwaves is rather complex and depends on snow properties like snow depth, density, and average grain size as well as the age of snowpack. With increasing temperature in spring, snow begins to melt and water covers the surface of snow pack which causes a sudden drop in backscatter. After snow melting period, soil and vegetation begin to thaw and consequently backscatter arise again. Figure 8 shows a typical example of freeze/thaw process as described above observable in ASCAT normalized backscatter at 40°. High diurnal difference of backscatter (green bars) implies frozen condition in the morning and thawing in the evening which can be used as an indicator of the transition between different phases.

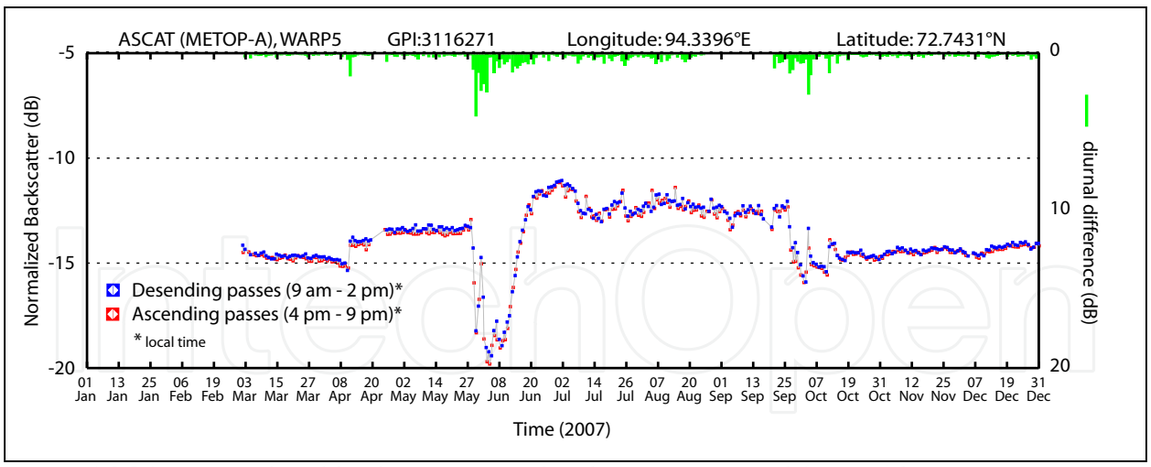

Fig. 8. ASCAT normalized backscatter at 40° indicating seasonal freeze/thaw process.

The high temporal sampling of the scatterometers in Polar Regions despite the frequent cloud cover and poor sunlight make them valuable instruments for sea ice observations. The sea ice imaging is based on the sensitivity of scatterometer to ice roughness and relatively high difference between the backscatter from open water and sea ice.
Long et al. (1999) used a simple linear function to approximate the backscatter at 40° (reference incidence angle):

$$\sigma^0(\theta) = A + B(\theta - 40) \tag{8}$$

where A is the σ^0 at 40° incidence and B describes the incidence angle dependency of backscatter.
The A and B parameters are calculated after combining the scatterometer observations from multiple passes from several days and using the Scatterometer Image Reconstruction (SIR) algorithm to enhance the resolution (Early et al., 2001). The A and B images represent the backscatter properties of the surface and are related to ice and snow characteristics over the imaging period (Long et al., 2001). Figure 9 illustrates examples of the normalized backscatter retrieved from ERS-1/2 scatterometer data available through the Scatterometer Climate Record Pathfinder (SCP) project (NASA-SCP).

7. Conclusion

C-band scatterometers have demonstrated to be valuable sensors for large-scale observation of the Earth's surface in a variety of disciplines. High temporal sampling in all weather conditions, multi-viewing capability and availability of long-term measurements make the European C-band scatterometers excellent Earth observation tools. Scatterometer data are used to extract geophysical parameters such as wind speed and direction, surface soil moisture, seasonal dynamics of vegetation, spatial and temporal variability of frozen train in high latitudes, snowmelt and sea ice. Furthermore the scatterometer data are utilized in hydrological modeling, observation of extreme events, flood and drought monitoring, and also used for climate change studies. The observations of the ERS-1/2 scatterometers

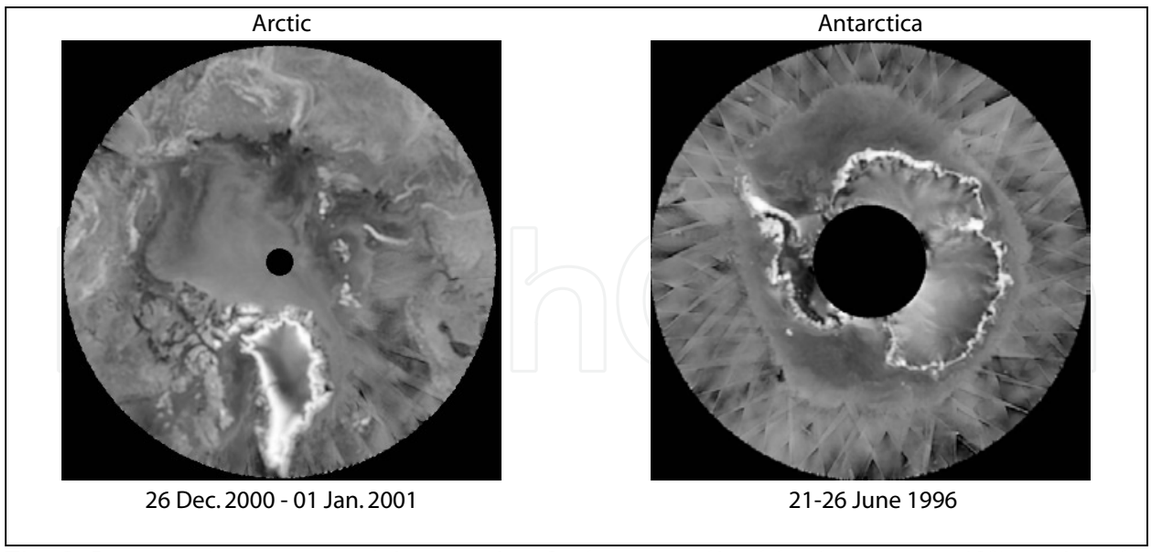

Fig. 9. Images of parameter *A* in equation-8 (the normalized backscatter at 40°) retrieved from ERS-2 scatterometer data after resolution enhancement. Adopted from (NSIDC).

(SCATs) together with the new series of advanced scatterometers (ASCAT) onboard Metop satellites ensure long-term global observation (from 1991 until at least 2020).

Acknowledgements

This work was supported by the geoland-II project in frame of the Global Monitoring for the Environment and Security (GMES), a joint initiative of European Commission (EC) and European Space Agency (ESA), and the Austrian Research Promotion Agency (FFG) through the Global Monitoring of Soil Moisture (GMSM) project.

8. References

ASCAT Product Guide v4 (2009), EUM/OPS-EPS/MAN/04/0028, EUMETSAT, Darmstadt, Germany, http://oiswww.eumetsat.org/WEBOPS/eps-pg/ASCAT/ASCAT-PG-0TOC.htm.

Attema E. P. W. and F. T. Ulaby (1978), Vegetation Modeled as a Water Cloud, Radio Science, Vol. 13, pp. 357.

Bartsch A., R. A. Kidd, W. Wagner and Z. Bartalis (2007), Temporal and spatial variability of the beginning and end of daily spring freeze/thaw cycles derived from scatterometer data, Remote Sensing of Environment, Vol. 106, pp. 360.

De Ridder K. (2000), Quantitative estimation of skin soil moisture with the Special Sensor Microwave/Imager, Boundary-Layer Meteorology, Vol. 96, pp. 421-432.

Doubkova M., V. Naeimi, W. Wagner and G. Henebry (2009), On the ability of the ERS scatterometer to detect vegetation properties, IEEE International Geoscience and Remote Sensing (IGARSS), Cape Town, South Africa, 12-17 July 2009.

Drinkwater M. R. and X. Liu (2000), Seasonal to interannual variability in Antarctic sea-ice surface melt, IEEE Transactions on Geoscience and Remote Sensing, Vol. 38, pp. 1827.

Drinkwater M. R., D. G. Long and A. W. Bingham (2001), Greenland snow accumulation estimates from satellite radar scatterometer data, Journal of Geophysical Research D: Atmospheres, Vol. 106, pp. 33935.

Early D. S. and D. G. Long (2001), Image reconstruction and enhanced resolution imaging from irregular samples, IEEE Transactions on Geoscience and Remote Sensing, Vol. 39, pp. 291.

EUMETCast, (accessed 2009), http://www.eumetsat.int/home/Main/What_We_Do/EUMETCast/index.htm.

FAO news report, (Accessed July 2009), http://www.fao.org/newsroom/en/news/2007/1000667.

Figa-Saldana J., J. W. Wilson, E. Attema, R. Gelsthorpe, M. R. Drinkwater and A. Stoffelen (2002), The advanced scatterometer (ASCAT) on the meteorological operational (MetOp) platform: A follow on for European wind scatterometers, Canadian Journal of Remote Sensing, Vol. 28, pp. 404-412.

Frison P. L. and E. Mougin (1996a), Monitoring global vegetation dynamics with ERS-1 wind scatterometer data, International Journal of Remote Sensing, Vol. 17, pp. 3201.

Frison P. L. and E. Mougin (1996b), Use of ERS-1 wind scatterometer data over land surfaces, IEEE Transactions on Geoscience and Remote Sensing, Vol. 34, pp. 550.

Frison P. L., E. Mougin and P. Hiernaux (1997), Observations and simulations of the ERS wind scatterometer response over a sahelian region, International Geoscience And Remote Sensing Symposium (IGARSS), pp. 1832-1834.

Geoland-II project, Integrated GMES project on land cover and vegetation, http://www.gmes-geoland.info/PROJ/index.php.

Hasenauer S., W. Wagner, K. Scipal, V. Naeimi and Z. Bartalis (2006), Implemetation of near real time soil moisture products in the SAF network based on METOP ASCAT data, paper presented at EUMETSAT Meteorological Satellite Conference, Helsinki, Finland, 12-16 June 2006.

Hersbach H., A. Stoffelen and S. De Haan (2007), An improved C-band scatterometer ocean geophysical model function: CMOD5, Journal of Geophysical Research C: Oceans, Vol. 112.

Huete A., K. Didan, T. Miura, E. P. Rodriguez, X. Gao and L. G. Ferreira (2002), Overview of the radiometric and biophysical performance of the MODIS vegetation indices, Remote Sensing of Environment, Vol. 83, pp. 195.

Jarlan L., P. Mazzega and E. Mougin (2002), Retrieval of land surface parameters in the Sahel from ERS wind scatterometer data: A "brute force" method, IEEE Transactions on Geoscience and Remote Sensing, Vol. 40, pp. 2056-2062.

Jarlan L., P. Mazzega, E. Mougin, F. Lavenu, G. Marty, P. L. Frison and P. Hiernaux (2003), Mapping of Sahelian vegetation parameters from ERS scatterometer data with an evolution strategies algorithm, Remote Sensing of Environment, Vol. 87, pp. 72-84.

Kimball J. S., K. C. McDonald, A. R. Keyser, S. Frolking and S. W. Running (2001), Application of the NASA scatterometer (NSCAT) for determining the daily frozen and nonfrozen landscape of Alaska, Remote Sensing of Environment, Vol. 75, pp. 113.

Klaes D. and K. Holmlund (2007), The EPS/Metop system: overview and first results, paper presented at Joint 2007 EUMETSAT Meteorological Satellite Conference and the 15th Satellite Meteorology & Oceanography Conference of the American Meteorological Society, Amsterdam, The Netherlands, 24-28 September 2007.

Le Hegarat-Mascle S., M. Zribi, F. Alem, A. Weisse and C. Loumagne (2002), Soil moisture estimation from ERS/SAR data: Toward an operational methodology, IEEE Transactions on Geoscience and Remote Sensing, Vol. 40, pp. 2647.

Liu W. T. (2002), Progress in scatterometer application, Journal of Oceanography, Vol. 58, pp. 121-136.

Long A. E. (1985), Towards a C-Band radar sea echo model for the ERS-1 scatterometer, Proceedings Conference on Spectral Signatures, Les Arcs, France, December 1985. European Space Agency Special Publication, ESA SP-247, 29-34.

Long D. G. and M. R. Drinkwater (1999), Cryosphere applications of NSCAT data, IEEE Transactions on Geoscience and Remote Sensing, Vol. 37, pp. 1671.

Long D. G. and M. R. Drinkwater (2000), Azimuth variation in microwave scatterometer and radiometer data over Antarctica, IEEE Transactions on Geoscience and Remote Sensing, Vol. 38, pp. 1857-1870.

Long D. G., M. R. drinkwater, B. Holt, S. Saatchi and C. Bertoia (2001), Global Ice and Land Climate Studies Using Scatterometer Image Data, EOS, Transaction of the American Geophysical Union, Vol. 82, pp. 503.

Magagi R. D. and Y. H. Kerr (1997), Retrieval of soil moisture and vegetation characteristics by use of ERS-1 wind scatterometer over arid and semi-arid areas, Journal of Hydrology, Vol. 188-189, pp. 361-384.

Magagi R. D. and Y. H. Kerr (2001), Estimating surface soil moisture and soil roughness over semiarid areas from the use of the copolarization ratio, Remote Sensing of Environment, Vol. 75, pp. 432-445.

Moeremans B. and S. Dautrebande (1998), Use of ERS SAR interferometric coherence and PRI images to evaluate crop height and soil moisture and to identify crops, Remote Sensing For Agriculture, Ecosystems, And Hydrology, Vol. 3499, pp. 9-19.

Moore R. K. and A. K. Fung (1979), Radar Determination Of Winds At Sea, Proceedings Of The Ieee, Vol. 67, pp. 1504-1521.

Moran M. S., D. C. Hymer, J. Qi and E. E. Sano (2000), Soil moisture evaluation using multi-temporal synthetic aperture radar (SAR) in semiarid rangeland, Agricultural and Forest Meteorology, Vol. 105, pp. 69.

Mougin E., A. Lopes, P. L. Frison and C. Proisy (1995), Preliminary analysis of ERS-1 wind scatterometer data over land surfaces, International Journal of Remote Sensing, Vol. 16, pp. 391.

NASA-EO, NASA's Earth observatory, (Accessed July 2009), http://earthobservatory. nasa.gov/NaturalHazards/category.php?cat_id=6.

NASA-SCP, The NASA Scatteromter Climate Record Pathfinder (SCP), http://www.scp.byu.edu/.

Naeimi V., C. Kuenzer, S. Hasenauer, Z. Bartalis and W. Wagner (2008), Evaluation of the influence of land cover on the noise level of ERS-scatterometer backscatter, International Geoscience and Remote Sensing Symposium (IGARSS), Barcelona, Spain. pp. 3685-3688.

Naeimi V., K. Scipal, Z. Bartalis, S. Hasenauer and W. Wagner (2009a), An Improved Soil Moisture Retrieval Algorithm for ERS and METOP Scatterometer Observations, IEEE Transactions on Geoscience and Remote Sensing, Vol. 47, pp. 555-563.

Naeimi V., (2009), Model improvements and error characterization for global ERS and METOP scatterometer soil moisture data, dissertation, pp. 111, Vienna University of Technology, Vienna.

Nghiem S. V. and W. Y. Tsai (2001), Global snow cover monitoring with spaceborne Ku-band scatterometer, IEEE Transactions on Geoscience and Remote Sensing, Vol. 39, pp. 2118.

NSIDC, National Snow and Ice Data Center, (Accessed July 2009), http://nsidc.org/data/nsidc-0260.html

Pulliainen J. T., T. Manninen and M. T. Hallikainen (1998), Application of ERS-1 wind scatterometer data to soil frost and soil moisture monitoring in boreal forest zone, IEEE Transactions On Geoscience And Remote Sensing, Vol. 36, pp. 849-863.

Quesney A., S. Le Hegarat-Mascle, O. Taconet, D. Vidal-Madjar, J. P. Wigneron, C. Loumagne and M. Normand (2000), Estimation of watershed soil moisture index from ERS/SAR data, Remote Sensing of Environment, Vol. 72, pp. 290.

Remund Q. P., D. G. Long and M. R. Drinkwater (2000), An iterative approach to multisensor sea ice classification, IEEE Transactions on Geoscience and Remote Sensing, Vol. 38, pp. 1843.

Stoffelen A. and D. Anderson (1997), Scatterometer data interpretation: Estimation and validation of the transfer function CMOD4, Journal of Geophysical Research C: Oceans, Vol. 102, pp. 5767-5780.

Ulaby F. T., R. K. Moore and A. K. Fung (1982), Microwave remote sensing: active and passive. Volume II. Radar remote sensing and surface scattering and emission theory.

UNESCO report (2006), United Nations World Water Developement Report 2, Water, a Shared Responsibility, p.121

Verhoef A. and Ad Stoffelen (2009), Validation of ASCAT 12.5-km winds, version 1.2, SAF/OSI/CDOP/KNMI/TEC/RP/147, EUMETSAT.

Wagner W. (1998), Soil Moisture Retrieval from ERS Scatterometer Data, dissertation, pp. 111, Vienna University of Technology, Vienna.

Wagner W., G. Lemoine, M. Borgeaud and H. Rott (1999a), A study of vegetation cover effects on ERS scatterometer data, IEEE Transactions on Geoscience and Remote Sensing, Vol. 37, pp. 938-948.

Wagner W., G. Lemoine and H. Rott (1999b), A method for estimating soil moisture from ERS scatterometer and soil data, Remote Sensing of Environment, Vol. 70, pp. 191-207.

Wismann V. (2000), Monitoring of seasonal snowmelt on Greenland with ERS scatterometer data, IEEE Transactions on Geoscience and Remote Sensing, Vol. 38, pp. 1821.

Wismann V. and K. Boehnke (1997), Monitoring snow properties on Greenland with ERS scatterometer and SAR, European Space Agency, (Special Publication) ESA SP. pp. 857-861.

Wismann V. R., K. Boehnke and C. Schmullius (1994), Global land surface monitoring using the ERS-1 scatterometer, International Geoscience and Remote Sensing Symposium (IGARSS), pp.1488.

Woodhouse I. H. and D. H. Hoekman (2000), Determining land-surface parameters from the ERS wind scatterometer, IEEE Transactions on Geoscience and Remote Sensing, Vol. 38, pp. 126-140.

Zine S., L. Jarlan, P. L. Frison, E. Mougin, P. Hiernaux and J. P. Rudant (2005), Land surface parameter monitoring with ERS scatterometer data over the Sahel: A comparison between agro-pastoral and pastoral areas, Remote Sensing of Environment, Vol. 96, pp. 438.

Geoscience and Remote Sensing New Achievements

Edited by Pasquale Imperatore and Daniele Riccio

ISBN 978-953-7619-97-8
Hard cover, 508 pages
Publisher InTech
Published online 01, February, 2010
Published in print edition February, 2010

Our planet is nowadays continuously monitored by powerful remote sensors operating in wide portions of the electromagnetic spectrum. Our capability of acquiring detailed information on the environment has been revolutionized by revealing its inner structure, morphology and dynamical changes. The way we now observe and study the evolution of the Earth's status has even radically influenced our perception and conception of the world we live in. The aim of this book is to bring together contributions from experts to present new research results and prospects of the future developments in the area of geosciences and remote sensing; emerging research directions are discussed. The volume consists of twenty-six chapters, encompassing both theoretical aspects and application-oriented studies. An unfolding perspective on various current trends in this extremely rich area is offered. The book chapters can be categorized along different perspectives, among others, use of active or passive sensors, employed technologies and configurations, considered scenario on the Earth, scientific research area involved in the studies.

How to reference

In order to correctly reference this scholarly work, feel free to copy and paste the following:

Vahid Naeimi and Wolfgang Wagner (2010). C-band Scatterometers and Their Applications, Geoscience and Remote Sensing New Achievements, Pasquale Imperatore and Daniele Riccio (Ed.), ISBN: 978-953-7619-97-8, InTech, Available from: http://www.intechopen.com/books/geoscience-and-remote-sensing-new-achievements/c-band-scatterometers-and-their-applications

INTECH
open science | open minds

InTech Europe
University Campus STeP Ri
Slavka Krautzeka 83/A
51000 Rijeka, Croatia
Phone: +385 (51) 770 447
Fax: +385 (51) 686 166
www.intechopen.com

InTech China
Unit 405, Office Block, Hotel Equatorial Shanghai
No.65, Yan An Road (West), Shanghai, 200040, China
中国上海市延安西路65号上海国际贵都大饭店办公楼405单元
Phone: +86-21-62489820
Fax: +86-21-62489821

IntechOpen